Available online at www.sciencedirect.com
SCIENCE DIRECT®
International Journal of Heat and Fluid Flow 24 (2003) 902–918
International Journal of HEAT AND FLUID FLOW
www.elsevier.com/locate/ijhff

Modeling of droplet entrainment phenomena at a quench front

M.J. Holowach, L.E. Hochreiter, J.H. Mahaffy, F.B. Cheung *

Department of Mechanical and Nuclear Engineering, The Pennsylvania State University, 137 Reber Building, University Park, PA 16802-1412, USA

Received 14 February 2003; accepted 15 May 2003

Abstract

The phenomena of droplet entrainment at a quench front is of practical importance as a clear understanding of the underlying mechanisms required to effectively calculate the interfacial mass, momentum, and energy transfer, which characterizes nuclear reactor safety, system design, analysis, and performance. The present study proposes a model for droplet entrainment at a quench front that is based on the best-understood physics related to the Lagrangian quenching phenomenon characteristic to light water reactor (LWR) safety analysis. The model is based on a film boundary layer and stability analysis that attempts to match the characteristic time and length scales of the entrainment phenomenon. This model has been developed such that direct implementation can be made into any two-phase flow simulation code with a three-field (continuous liquid, droplet, and vapor) flow model. Comparisons with integrated transient test data independent of those used for model development have been performed to verify the applicability of the proposed model for the prediction of the entrainment rate of liquid droplets at a quench front under typical reflood conditions envisioned in LWRs.

Keywords: Droplet entrainment; Quench front; Safety analysis

1. Introduction

It is widely recognized that the entrainment of liquid droplets by a gas flow is of considerable practical importance for the effective modeling of heat and mass transfer processes in two-phase systems (Ishii and Grolmes, 1975). The mechanisms of interfacial mass, momentum, and energy transfer between phases are significantly altered by the entrainment of liquid. The entrainment of liquid can occur under nuclear reactor safety analysis considerations due to two distinctly different situations in upward co-current two-phase vertical flow. Droplet entrainment can result from situations in which a gas is flowing over a liquid film such as in annular film flow, as well as occurring at a quench front or within a froth region when vapor bubbles up through a pool, and/or vapor is being generated due to the quenching phenomenon as shown in Fig. 1. A detailed analysis and model development for the first case, annular film flow droplet entrainment, has been previously published by Holowach et al. (2002). The present study focuses on the second situation, which is the entrainment of droplets at a quench front.

The critical heat flux (CHF) and post-critical heat flux (post-CHF) in light-water cooled reactors as well as the effectiveness of emergency core cooling systems in water reactors are all significantly affected by the entrainment of liquid droplets in the vapor core flow (Ishii and Grolmes, 1975). In the case of a transient thermal hydraulic systems analysis computer code utilized for such nuclear reactor safety calculations, there is a need to accurately calculate droplet entrainment for the geometrical configuration that is modeled with a thermal hydraulic node scheme. Additionally, since many two-phase flow processes are time-varying in nature, there is a necessity to develop a droplet entrainment model that is based on fundamental physics and has the requisite flexibility to be used in transient system calculations that include the modeling of a quench front, which is inherently Lagrangian in nature.

When modeling the entrainment rate at a quench front, many of the macroscopic-parameter based models currently available in the open literature are not developed to predict the droplet entrainment rate, but

* Corresponding author. Tel.: +1-814-863-4261; fax: +1-814-863-8682.
E-mail address: fxc4@psu.edu (F.B. Cheung).

0142-727X/$ - see front matter © 2003 Elsevier Inc. All rights reserved.
doi:10.1016/S0142-727X(03)00085-7

Nomenclature

A_{cv}	the interfacial area in the control volume
$A_{entr,w}$	frontal area of wave crest
A_F	flow area
A_{int}	interfacial area
A_{wall}	cross-sectional area of tube wall (for stored energy calculations)
$C_{p,water}$	specific heat of water
$C_{p,wall}$	specific heat of the wall
D_{drop}	droplet diameter in quench front entrainment model
D_H	hydraulic diameter
D_{jet}	liquid jet diameter
G_g	vapor mass flux
G_e	entrained mass flux
h_{fg}	enthalpy of vaporization
$\dot{m}_{aqf}$	mass flow rate just above the quench front
$\dot{m}_{entr}$	entrained mass flow rate just above the quench front
$\dot{m}_{in}$	channel inlet mass flow rate
$\dot{m}_{vap}$	vapor mass flow rate just above the quench front
$\dot{m}_{vap,bqf}$	vapor mass flow rate generated below the quench front
$\dot{m}_{vap,qf}$	vapor mass flow rate generated at the quench front
P_H	heated perimeter
P_w	wetted perimeter
q'	linear heat rate
Re^*	critical film Reynolds number (Hsu and Westwater, 1960)
$Re_{vap,gen}$	Reynolds number (based on quench front vapor generation)
S_E	droplet entrainment flux (mass flow rate per unit interfacial area, kg/m^{2}s)
T_{sat}	saturation temperature
T_q	quench temperature (usually minimum film boiling temperature)
$T_{w,cv}$	period of phenomena reflood entrainment control volume
U_q	quench front velocity
$U_{vap,bqf}$	characteristic vapor velocity for vapor generated below the quench front
$U_{vap,crit}$	critical vapor velocity due to quench front vapor generation
$V_{entr,d}$	the volume of liquid entrained in a single droplet
w_g	vapor mass flow rate
w_e	entrained droplet mass flow rate
y^*	critical vapor film thickness
z_q	quench front elevation

Greeks

α_l	volume fraction occupied by continuous liquid
α_q	void fraction just below the quench front
Γ	local vapor generation rate
λ	wavelength
λ_{crit}	critical wavelength
μ	dynamic viscosity
ν	kinematic viscosity
ρ	density
ρ_l	local liquid density
ρ_q	two-phase density just below the quench front
ρ_{wall}	cold density of the wall (for stored energy calculations)
$\tau_{w,cv}$	period of the entrainment phenomena in the control volume

Subscripts

crit	critical (wavelength)
cv	control volume
e	entrained
f	fluid
g	vapor
q	quench front

rather an equilibrium entrained droplet fraction above a pool. As a result, these models are of limited use in a computer code calculation that requires the calculation of the local entrainment rate of liquid droplets in a confined space (i.e. a nuclear reactor subchannel) as compared to an open space (i.e. pool with gas bubbling up through it).

This work presents the process utilized for the development of a physical model to predict the rate of droplet entrainment at a quench front/froth region by first summarizing the task of reducing experimental data to a form that can be readily used for model development. Then, a physical model has been developed utilizing a combination of the underlying physics and the reduced experimental data. In order to obtain suitable data for physical model development, results from fundamental tests in easily quantified geometries were required as more complex prototypical tests generally yield data that can be more difficult to reduce to quantify a single phenomenon such as droplet entrainment rate at a quench front.

For example, several reflood tests like the FLECHT SEASET series (Lee et al., 1982) have been conducted utilizing rod bundle geometries with spacer grids so as to

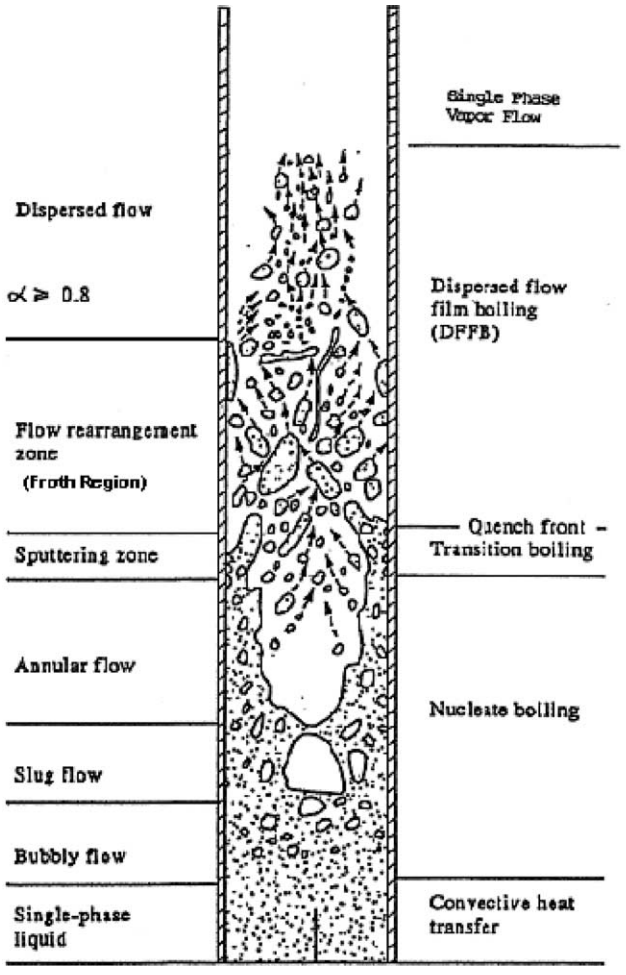

Fig. 1. Heat transfer and fluid flow phenomena in a bottom reflood scenario.

provide a scalable prototypical model to an actual pressurized water reactor (PWR) fuel rod bundle design. Additionally, reflood tests have been performed in simpler cylindrical tube geometries such as the RE-FLEX (Denham et al., 1980; Denham, 1981) and the University of California at Berkeley (UCB) series of tests (Seban et al., 1978; Seban and Greif, 1983; Ng and Banerjee, 1983). The simpler cylindrical tube tests can more readily be applied to fundamental model development (i.e. entrainment, dispersed flow film boiling, interfacial heat transfer and drag, etc.) since data from these tests can much more easily be reduced, whereas a rod bundle test that can have cross-flows between channels and significant heat transfer and flow effects brought on by the presence of spacer grids presents much more complexity for the reduction of such parameters as the entrainment rate at a quench front. Though, for safety analysis reasons, it is important to consider the effects of spacer grids, cross-flows, radial power distributions, etc., at the initial stage of a fundamental physical model development effort (i.e. entrainment model development) starting with data from basic experimental investigations is the most efficient means at identifying and quantifying the parametric effects of a particular phenomenon.

The progression of this work starts with the derivation and application of a method to reduce fundamental reflood test data to build a database of quench front droplet entrainment rate data. Then, a control volume physical model for quench front droplet entrainment is developed based on modeling the postulated phenomena and parametric effects such that characteristic time scales and length scales are preserved for the quench front entrainment phenomena. The physical model is then compared to the entrainment rate database, such that suitable parametric corrections are identified thus yielding a physical model with sufficient flexibility accounting for the separate effects of parameters. Subsequent comparisons of FLECHT SEASET integral effects experimental reflood data with predictions from the COBRA-TF thermal hydraulic systems analysis computer code (upgraded with the proposed quench front entrainment model) have been performed in order to show the validity and applicability of the proposed model.

2. Utilization of existing entrainment data

In order to estimate the droplet entrainment rate at a Lagrangian quench front utilizing existing fundamental single-tube reflood heat transfer experimental data, a methodology has been developed to perform a mass balance at the quench front such that the droplet entrainment rate can be estimated. The underlying stipulation is that this method of data reduction can readily be applied to current sets of experimental data that are primarily comprised of wall thermocouple readings, inlet flow rates, applied linear heat rates, and exit pressure.

A mass balance on a control volume characterizing the region from the tube inlet up to the quench front, shown in Fig. 2, has been developed and applied such that the entrained droplet mass flow rate at the quench front can be estimated. A similar methodology was employed in the reduction of the PWR FLECHT SEASET reflood experimental data (Lee et al., 1982). An overall mass balance on the control volume is written as

$$\underset{(1)}{\dot{m}_{\mathrm{aqf}}} = \underset{(2)}{\dot{m}_{\mathrm{in}}} - A_{\mathrm{F}} \underset{(3)}{\frac{\mathrm{d}}{\mathrm{d}t}} \int_0^{z_{\mathrm{q}}} \rho \, \mathrm{d}z \tag{1}$$

For the above relation, $\dot{m}_{\mathrm{aqf}}$ = mass flow rate just above the quench front, z_{q} = quench front elevation, A_{F} = flow area and $\dot{m}_{\mathrm{in}}$ = calculational channel inlet mass flow rate.

In Eq. (1), term 1 represents the mass flow rate out of the control volume (above the quench front), term 2 represents the mass flow rate into the control volume, and term 3 represents the mass storage within the con-

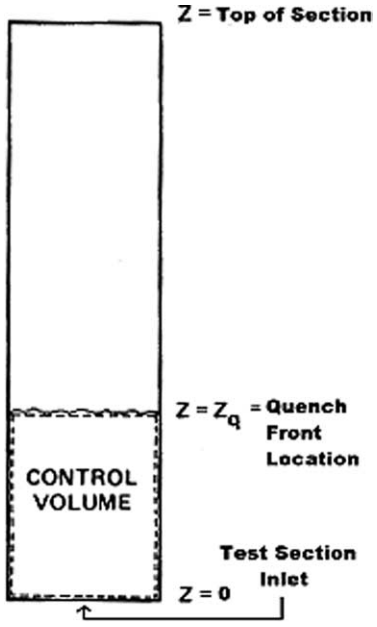

Fig. 2. Control volume for quench front mass balance.

trol volume (primarily due to the control volume size expanding due to quench front translation with the inlet being fixed).

We assume that the mass flow rate above the quench front is composed of both a combination of entrained and vapor phases. The vapor is generated below the quench front by boiling heat transfer, and the vapor generated at the quench front is due to quenching action. The mass flow rate above the quench front is written as

$$\dot{m}_{\mathrm{aqf}} = \dot{m}_{\mathrm{entr}} + \dot{m}_{\mathrm{vap}} = \dot{m}_{\mathrm{entr}} + \dot{m}_{\mathrm{vap,bqf}} + \dot{m}_{\mathrm{vap,qf}} \tag{2}$$

For the above relation, $\dot{m}_{\mathrm{entr}}$ = entrained mass flow rate just above the quench front, $\dot{m}_{\mathrm{vap}}$ = vapor mass flow rate just above the quench front, $\dot{m}_{\mathrm{vap,bqf}}$ = vapor mass flow rate generated below the quench front and $\dot{m}_{\mathrm{vap,qf}}$ = vapor mass flow rate generated at the quench front.

Since the upper boundary of the control volume established for this analysis moves with time due to quench front translation, and the lower level of the control volume is at a fixed inlet height, $z = 0$, Eq. (1) can be rewritten utilizing the Leibnitz formula

$$\dot{m}_{\mathrm{aqf}} = \dot{m}_{\mathrm{in}} - A_{\mathrm{F}}\rho_{\mathrm{q}}\frac{\mathrm{d}z_{\mathrm{q}}}{\mathrm{d}t} - A_{\mathrm{F}}\int_0^{z_{\mathrm{q}}}\frac{\mathrm{d}\rho}{\mathrm{d}t}\,\mathrm{d}z \tag{3}$$

In the above relation, ρ_{q} represents the two-phase density just below the quench front. For cases where the liquid density is significantly greater than the vapor density, this can be estimated in terms of the void fraction just below the quench front, α_{q}, and the local liquid density, ρ_{l}

$$\rho_{\mathrm{q}} \approx (1-\alpha_{\mathrm{q}})\rho_{\mathrm{l}} \tag{4}$$

Additionally, the term $\mathrm{d}z_{\mathrm{q}}/\mathrm{d}t$ is equal to the quench front velocity, U_{q}. Furthermore, consistent with the observations in the FLECHT SEASET experiments (Lee et al., 1982) the assumption can be made that the time rate of change of density in the calculational channel is small except near the quench front. Utilizing these assumptions and definitions, the quench front mass balance is rewritten to yield an expression for the entrained flow rate above the quench front

$$\dot{m}_{\mathrm{entr}} = \dot{m}_{\mathrm{in}} - \dot{m}_{\mathrm{vap,bqf}} - \dot{m}_{\mathrm{vap,qf}} - A_{\mathrm{F}}(1-\alpha_{\mathrm{q}})\rho_{\mathrm{l}}U_{\mathrm{q}} \tag{5}$$

Note that the mass balance presented in Eq. (5) inherently assumes a constant inlet flow rate, and no cross-flow into or out of the calculational channel below the quench front. This could possibly be a poor assumption in a rod bundle configuration where a cross-flow can be induced by such effects as the radial power shape, pressure drop, and flow restrictions. However, for the case of the analysis of a single enclosed tube reflood case, such as the UCB (Seban et al., 1978; Seban and Greif, 1983; Ng and Banerjee, 1983) and REFLEX (Denham et al., 1980; Denham, 1981) experiments where cross-flow is not possible, this is a reasonable assumption as long as the inlet mass flow rate is nearly constant with time.

Vapor may or may not be generated below the quench front for a particular reflood case and quench front location depends on the subcooling and the axial power shape. However, by making the assumption of thermodynamic equilibrium in the flow below the quench front, the vapor mass flow rate due to vapor being generated below the quench front at locations above the saturation line is calculated by

$$\dot{m}_{\mathrm{vap,bqf}} = \frac{\int_0^{z_{\mathrm{q}}} q'\,\mathrm{d}z - \dot{m}_{\mathrm{in}}C_{p,\mathrm{water}}\Delta T_{\mathrm{sub}}}{h_{\mathrm{fg}}} \tag{6}$$

In the above relation, q' = linear heat rate, $C_{p,\mathrm{water}}$ = specific heat of the water, ΔT_{sub} = inlet subcooling, and h_{fg} = enthalpy of vaporization.

Note that the underlying assumption in Eq. (6) is that the flow below the quench front is considered to be in thermodynamic equilibrium. For cases of subcooled boiling heat transfer with significant vapor generation, the validity of Eq. (6) decreases. It is postulated that the use of Eq. (6) for this model development is valid, as it appears that the vapor generation at the quench front due to quenching action has a dominant effect on the droplet entrainment at the quench front.

The vapor generated at the quench front due to quenching action is approximated by assuming average thermal properties for the tube wall and by assuming that all heat released during the quenching process contributes directly to vapor generation with vapor properties at saturation conditions. The former is a good assumption since the tubes used for fundamental reflood tests (such as UCB and REFLEX) are constructed of a single material with well-known thermal properties, and the latter is generally a good

assumption, as the vapor generation at a quench front is a rapid process that can be postulated as a non-equilibrium thermodynamic process for cases in which subcooled liquid conditions exist at the quench front. It is acceptable to assume that vapor generated at the location of the quench front is at saturation temperature, since minimal superheating of the vapor can occur in the generally small axial region that encompasses the quench/froth region. The estimated vapor generation due to quenching, utilizing these assumptions, is given as

$$\dot{m}_{\mathrm{vap,qf}} = \frac{\rho_{\mathrm{wall}} C_{p,\mathrm{wall}} A_{\mathrm{wall}} (T_{\mathrm{q}} - T_{\mathrm{sat}}) U_{\mathrm{q}}}{h_{\mathrm{fg}}} \tag{7}$$

Eqs. (6) and (7) can now be utilized to arrive at the respective vapor flow rates such that they may be substituted into Eq. (5) for the solution of the estimated entrained mass flow rate at the quench front. In an effort to provide closure to the series of equations in this analysis, and subsequently solve Eq. (5) for the entrained flow rate at the quench front, the parameters identified in Table 1 must be known.

For fundamental tube reflood experiments, items 1 through 7 in Table 1 are readily determined utilizing measured test boundary conditions (inlet flow conditions, applied power shape, thermal properties) and normally measured parameters (i.e. wall temperature and pressure). The quench temperature can be easily determined by examination of individual thermocouple readings over time, and, the quench front velocity can be estimated by taking the slope of a curve representing the quench front location versus time. Such a curve is generated by plotting the quench front height versus time from observation of the quench times for a series of thermocouples at over a range of axial heights.

With the exception of a very small number of cases where gamma densitometer estimates of void fraction at the quench front were obtained (Ng and Banerjee, 1983), there is no other data available in the open literature which includes measurements of the void fraction directly below the quench front for fundamental tube reflood experiments. Therefore, item 8 in Table 1 remains an unknown for most cases. It appears that a reasonable estimation of the void fraction below the quench front is very complex since there are many effects and parameters which have a strong effect on this local void fraction (i.e. subcooling, pressure, flow regime, flow rates, axial conduction, heat flux) below this Lagrangian front. In order to make an initial estimate at handling this unknown such that the reduction of fundamental single-tube reflood test data can proceed, the value of the void fraction just below the quench front is ranged between 0 and 1, such that a "ranged" droplet entrainment rate may be determined. By plotting the values of the entrained droplet mass flow rate in error bar form (to represent the range of possible droplet entrainment rates due to the possible range of void fractions just below the quench front), analysis and model development utilizing trend assessment can be conducted for a range of conditions.

Table 1
Experimental quantities that must be known to solve for the entrained mass flow rate at the quench front

Item #	
1	The inlet mass flow rate and subcooling
2	The location of the quench front
3	The power supplied to the flow below the quench front
4	The liquid and wall thermal properties
5	The quench temperature
6	The quench front velocity
7	The pressure
8	The void fraction just below the quench front

2.1. Analysis of test data

Data from three series of tests conducted at the University of California at Berkeley (Seban et al., 1978; Seban and Greif, 1983; Ng and Banerjee, 1983) and data from two series of the REFLEX tests conducted by the United Kingdom Atomic Energy Authority at Winfrith (Denham et al., 1980; Denham, 1981) were selected for evaluation. Experimental runs were selected for which the quench temperature was approximately equal to the minimum film boiling temperature, and where the quench front flow regime was not annular flow, but rather a froth region. The froth region is defined as the region above the quench front where a mixture of droplets, slugs, and ligaments exist due to the vapor generation and disturbances at the quench front. Cases with quench temperatures below the minimum film boiling temperature were excluded from this model development since they do not directly represent the quench front phenomena characteristic to a conventional light water reactor design.

In the experimental reflood heat transfer runs examined, a range of pressures, temperatures, flow rates, and quench front energy release rates were considered for the model development. The individual test section geometries for the given experimental data are summarized in Table 2. From Table 2, it can be seen that the inside tube diameters roughly approximate the hydraulic diameter of both PWR and boiling water reactor flow subchannels. Additionally, a range of representative amounts of stored energy is considered with this data set since there are a range of wall thicknesses in the different experimental setups. Further calculations show that the range of quench front energy release rates in the selected sets of experimental data encompasses the prototypical quench front energy release rate at the quench front in a traditional PWR post-LOCA (loss of coolant accident) reflood transient and available integrated effects test data such as the FLECHT SEASET series of experimental tests (Lee et al., 1982).

Table 2
Test section geometrical parameters ((A)—Seban and Greif, 1983, (B)—Denham et al., 1980, (C)—Denham, 1981, (D)—Seban et al., 1978 and (E)—Ng and Banerjee, 1983)

Test reference	Material	Inside diameter (mm)	Wall thickness (mm)	Height (m)
REFLEX [B, C]	Inconel 600	12.56	1.66	3.95
UCB [A]	Inconel 600	14.25	0.83	3.66
UCB [D & E]	Inconel 600	14.40	0.76	3.66

The selected sets of test data were analyzed and reduced to determine a range of quench front entrainment rates utilizing the methods developed in this section. For cases in which the void fraction just below the quench front was not known, the void fraction was ranged between 0 and 1 to obtain the results that are presented in Table 3. For the cases where the void fraction just below the quench front was known by gamma densitometer readings (Ng and Banerjee, 1983), an estimated entrainment rate is given instead of a range of entrainment rates, with the results of these analyses presented in Table 4. Both summary tables show the range of test conditions analyzed including the cold fill rate, pressure, inlet mass flow rate, calculated equilibrium quality at the quench front, calculated vapor mass flow rate generated below the quench front, calculated vapor mass flow rate generated at the quench front, quench front velocity, and entrainment rates represented as mass fluxes.

Since this wide range of test data has been reduced and put in a useful form, it can be applied to the development of a fundamental quench front droplet entrainment model and extrapolated for the use in calculation of droplet entrainment in the reflood phenomenon in rod bundles. Though it may appear at first glance that the geometrical confines of reflood in a single tube are not representative of droplet entrainment in rod bundles, it is postulated that fundamental tube quench data can be applied to better model the actual quenching phenomenon than most currently-used entrainment models (Kataokoa and Ishii, 1983) which are based on modeling droplet entrainment in large diameter pools. Large diameter pools do not exhibit the prototypical ratio of heated perimeter to flow area that is characteristic to both rod bundle and heated tube configurations. Subsequent analysis of the parametric effects of the postulated phenomenon, and comparison to this reduced experimental data in the following sections show the usefulness of this "ranged" data for the development of a fundamental quench front droplet entrainment model.

3. Quench front entrainment model development

Based on the success of the modeling the droplet entrainment rate in annular two-phase flow utilizing a control volume and Kelvin–Helmholtz stability analysis (Holowach, 2002), a similar means of phenomena characterization and evaluation is employed in the development of the quench front entrainment model. To successfully accomplish this goal, parametric effects as well as characteristic time scales and length scales must be correctly modeled so as to effectively calculate the droplet entrainment over a range of flow, heat release, and pressure conditions.

In the annular flow entrainment model, developed by Holowach (2002), the primary characteristic length scale was taken to be that of the Kelvin–Helmholtz instability for the calculation of the wave geometry and estimation of the control volume characteristics. This selection of length scale was based on the experimental observations of Woodmansee and Hanratty (1969). Due to the complexity and randomness of the quenching phenomenon in a confined space, no detailed visual observations are available which clearly depict length and time scales, therefore, length scales, time scales, and characteristic phenomena must be postulated based on similar, yet simplified phenomena which have been observed and quantified. Examples of such phenomena include annular film entrainment and film boiling. In modeling the quench front entrainment phenomenon, it is postulated that the Kelvin–Helmholtz instability length scale is of particular significance in the wave action that results in the droplet formation and entrainment. Additionally, another length scale of particular interest is the vapor film thickness near the wall during the quenching process. Also, due to postulated liquid jet formations brought on by the quench front vapor generation, the Rayleigh characterization of the breakup of a quasi-static jet will be useful in the particular length scale quantification which is discussed in detail by Wallis (1969).

By performing a control volume analysis on the region of the calculational channel that includes the quench front and froth region, a general expression can be formed for the droplet entrainment rate at the surface of the froth region. The droplet entrainment rate is postulated to be a function of the volume of liquid swept off of each wave that is developed, the wavelength, the number of waves in the control volume, and the velocity at which the waves travel through the control volume. A side-view schematic of the postulated droplet entrainment mechanism, characteristic velocities, and characteristic length scales that are included in the following discussions is presented in Fig. 3. The general expression for the droplet entrainment mass flux at the top of the froth front, which is similar to the base expression for

Table 3
Reduced test parameters for cases in which the void fraction just below the quench front was not measured ((A)—Seban and Greif, 1983, (B)—Denham et al., 1980, (C)—Denham, 1981 and (D)—Seban et al., 1978)

Ref.	Run ID	Cold fill rate (mm/s)	Pressure (MPa)	Inlet mass flow rate (kg/s)	Calculated quality at the quench front (%)	Mass flow rate of vapor generated below the quench front (kg/s)	Mass flow rate of vapor generated at the quench front (kg/s)	Quench front velocity (mm/s)	Entrained mass flux $\alpha = 0$ (kg/m^2 s)	Entrained mass flux $\alpha = 1$ (kg/m^2 s)
[A]	3073–4	76.2	0.2	0.0120	−10.7	0	0.000625	38.1	35.81	70.01
[A]	3073–8	76.2	0.2	0.0120	−6.1	0	0.000652	38.1	35.67	69.82
[A]	3070–4	76.2	0.3	0.0119	−10.4	0	0.000574	38.1	34.35	69.48
[A]	3070–8	76.2	0.3	0.0119	−5.7	0	0.00058	38.1	34.30	69.43
[A]	3076–8	76.2	0.1	0.0121	−5.2	0	0.000389	23.1	51.42	72.51
[A]	3053–4	25.4	0.3	0.0040	1.2	4.77E−05	0.000221	14.5	9.93	22.75
[B]	129–2	159	0.2	0.0192	−8.4	0	0.001043	27.2	121.14	145.56
[B]	129–9	159	0.2	0.0192	−6.8	0	0.000931	24.1	124.96	146.64
[A]	3051–8	25.4	0.2	0.0040	16.8	0.000675	0.000227	3.81	16.00	19.42
[A]	3058–4	76.2	0.2	0.0120	−2.8	0	0.00058	11.7	61.16	71.68
[C]	01×107–2	43.1	0.4	0.0052	−12.0	0	0.000393	11.9	27.79	38.36
[C]	01×107–6	43.1	0.4	0.0052	−6.0	0	0.000425	18.5	21.53	37.77
[C]	01×107–13	43.1	0.4	0.0052	−4.0	0	0.000468	20.1	19.77	37.38
[C]	01×092–2	40.0	0.4	0.0048	−2.0	0	0.000413	9.40	27.06	35.72
[D]	187	24.6	0.1	0.0040	6.0	0.000312	0.000121	3.81	18.35	21.75
[D]	181	25.1	0.1	0.0040	13.0	0.000676	8.08E−05	2.03	25.59	27.39
[D]	125	73.9	0.1	0.0118	−1.0	0	0.000268	9.91	21.12	30.04
[D]	194	75.2	0.1	0.0121	1.0	5.2E−05	0.000147	2.79	28.31	30.81
[D]	137	76.2	0.1	0.0121	9.0	0.000468	0.00015	3.05	25.53	28.21
[D]	136	127	0.1	0.0202	3.0	0.000156	0.000165	3.05	27.32	30.04
[D]	135	175	0.1	0.0278	0.7	3.64E−05	0.000166	3.56	27.52	30.75

Table 4
Reduced test parameters for cases in which the void fraction just below the quench front was measured (Ng and Banerjee, 1983)

Run ID	Cold fill rate (mm/s)	Pressure (MPa)	Inlet mass flow rate (kg/s)	Calculated quality at the quench front (%)	Mass flow rate of vapor generated below the quench front (kg/s)	Mass flow rate of vapor generated at the quench front (kg/s)	Quench front velocity (mm/s)	Entrained mass flux (kg/m^2s)
14-3-80	76.2	0.1	0.0123	4.3	0.000523	0.000308	2.62	71.92
10-1-80	25.4	0.1	0.0041	12.5	0.000513	0.000115	3.7	19.08
10-1-80	25.4	0.1	0.0041	13.9	0.000979	0.000128	4.17	22.02

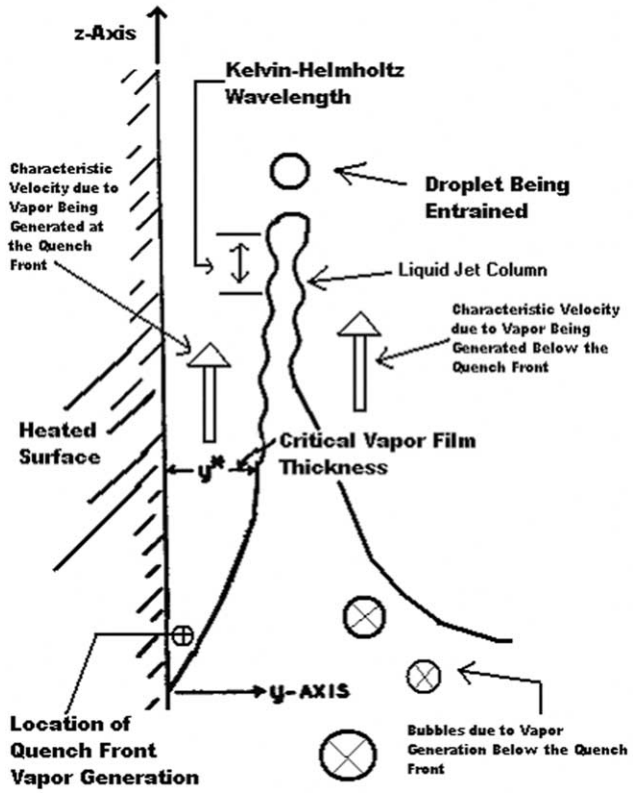

Fig. 3. Postulated mechanisms, characteristic velocities, and characteristic length scales for the quench front/froth front entrainment phenomenon.

the entrainment rate in the annular entrainment model presented by Holowach (2002), is given as

$$S_E = \frac{V_{entr,d}\rho_f N_{w,cv}}{A_{cv}T_{w,cv}} \tag{8}$$

In the above equation, S_E = droplet entrainment flux (entrainment rate per unit interfacial area, kg/m^2s), $V_{entr,d}$ = volume of liquid entrained in a single droplet, ρ_f = liquid density, $N_{w,cv}$ = number of waves in the control volume, A_{cv} = interfacial area in the control volume and $T_{w,cv}$ = period of the entrainment phenomena in the control volume.

Since quench front propagation can be assumed to be one-dimensional on average, the interfacial area, characterizing the area normal to the top of the froth region within the control volume (A_{cv}) is postulated to be simply equal to the flow area

$$A_{cv} = A_F \tag{9}$$

In order to characterize the length scale of the Kelvin–Helmholtz wave and the period of the entrainment phenomena, a local characteristic vapor velocity must be estimated. The local vapor generation due to heat transfer at a quench front is readily calculated in a finite difference thermal hydraulic systems analysis codes utilizing heat transfer coefficients determined from the

construction of a continuous boiling curve over a range of heat transfer regimes. With the calculated vapor generation due to quenching action, a characteristic vapor velocity can be calculated knowing the vapor density (which can be assumed to be the saturation density), and a characteristic flow area that can be estimated utilizing a characteristic length scale. Therefore, a geometrical constraint (length scale) must be assumed for which the vapor is formed and exits the quench region in order to calculate a local vapor velocity. There is some inherent error in assuming saturation properties at the quench front region since the wall temperature in at least a portion of this region is above the saturation temperature, but this is believed to be an acceptable assumption since it can be postulated that there is a small amount of vapor superheating at the quench front due to the relatively small distance over which this region exists, along with the relatively high vapor velocities (i.e. short vapor residence time) in this region.

Due to the similarity of the quenching phenomena with that of a developing vapor film in the film boiling phenomenon, it can be postulated that the geometrical constraint through which the vapor must flow is characterized by the critical thickness for the vapor film. Knowing the heated perimeter and the critical thickness for the vapor film, a characteristic flow area can be calculated such that a characteristic velocity for quench front vapor generation can subsequently be determined. A theoretical means for calculating the critical thickness for the vapor film that is created at a wall in vertical film boiling has been proposed by Hsu and Westwater (1960). The Hsu and Westwater model is based on the theoretical dependence of the film velocity and that of the film thickness (in the y-direction). A sketch of the film boiling model and associated dimensions postulated by Hsu and Westwater (1960) is given in Fig. 4. The critical vapor film thickness, y^*, calculated in Hsu and Westwater's model is given in terms of a critical Reynolds number and fluid properties as

$$y^* = \left[\frac{2\mu_g^2 Re^*}{g\rho_g(\rho_l - \rho_g)}\right]^{1/3} \tag{10}$$

$$Re^* = \frac{y^* u^* \rho_g}{\mu_g} \tag{11}$$

The critical vapor Reynolds number, Re^*, signifies the transition between viscous and turbulent vapor film flow in the film boiling model proposed by Hsu and Westwater (1960). This critical Reynolds number is estimated to be equal to a value of 100, and this estimation is supported by Rohsenow's computations (Rohsenow et al., 1953) of values ranging from 80 to 120 for the critical vapor Reynolds number during film condensation on vertical surfaces in the presence of large shear stresses. The critical Reynolds number is defined in terms of the maximum vapor velocity, u^*, existing at the critical height where the film flow transitions to turbulent flow.

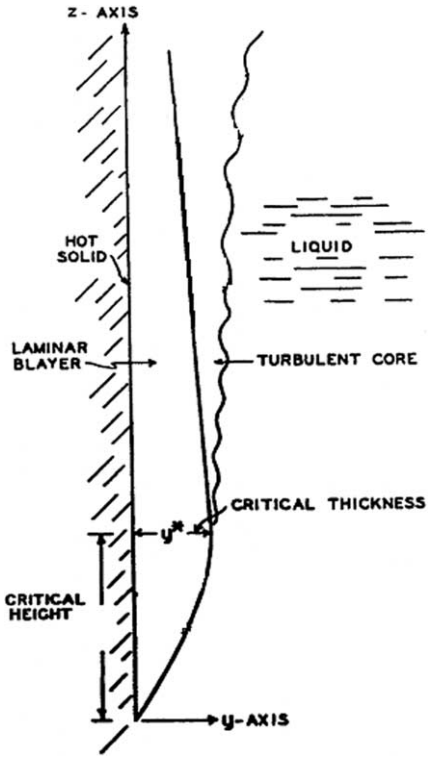

Fig. 4. Postulated film boiling geometrical model presented by Hsu and Westwater (1960).

For conventional PWR applications, the vapor film thickness is expected to be small with respect to the flow subchannel hydraulic diameter based on the experimental findings presented by Hsu and Westwater (1960). Therefore, the local critical vapor velocity at the quench front due to vapor generation from quenching action is subsequently estimated in terms of the local vapor generation rate, Γ, and the heated perimeter, P_H, as

$$U_{vap,crit} = \frac{\Gamma}{\rho_g P_H y^*} \tag{12}$$

Utilizing the basis of the Kelvin–Helmholtz instability for the droplet formation process, the critical wavelength, λ_{crit}, which represents the characteristic wavelength for droplet formation, can now be calculated utilizing the characteristic vapor velocity that was determined utilizing the critical film thickness approximation. It is postulated that the droplets entrained at the top of the froth front are formed by the action of the high vapor film velocity and subsequent instabilities. The critical wavelength that is postulated to characterize this phenomenon is calculated using a simplified Kelvin–Helmholtz estimation (Hewitt and Hall-Taylor, 1970)

$$\lambda_{crit} = \frac{2\pi\sigma g_c}{\rho_g U_{vap,crit}^2} \tag{13}$$

The period of the entrainment phenomena in the control volume ($T_{w,cv}$) is estimated by developing a characteristic time scale for the vapor flowing over the liquid ligaments which deform as a result of the instability and shearing forces. Since, it is postulated that vapor generated below the quench front has some impact on the droplet entrainment rate at the quench front, this time scale should account for both transport processes (vapor flow through the film along the wall due to quench front vapor generation and vapor flow through the center portion of the calculational subchannel due to vapor generation below the quench front).

The characteristic velocity for vapor generated below the quench front is defined by the following expression which adjusts the effective flow area for vapor generated below the quench front by subtracting the area taken up by the vapor film along the heated wall from the total flow area. This determines an effective flow area for the vapor generated below the quench front such that a characteristic velocity for the below quench front vapor generation may be calculated. Therefore, the characteristic vapor velocity for vapor generated below the quench front is given as

$$U_{vap,bqf} = \frac{\dot{m}_{vap,bqf}}{\rho_g (A_F - P_H y^*)} \tag{14}$$

The characteristic time scale for the transport of entrained droplets out of the control volume can now be postulated by considering the vapor flow in the film along the wall due to vapor generation at the quench front and that of the vapor flow due to vapor generation below the quench front. Since the time scale for droplets leaving the control volume is related to the droplet interfacial drag caused by vapor flow, it is postulated that the characteristic time scale is related to the average of the squared values of the below quench front and film vapor velocities. Based on this assumption, the time period for the control volume is postulated to be

$$T_{w,cv} = \frac{\lambda_{crit}}{(1/2)(U^2_{vap,crit} + U^2_{vap,bqf})^{1/2}} \tag{15}$$

The breakup of a liquid jet is a classical problem that was studied by Rayleigh, where it was determined that the most unstable wavelength is about 4.5 times the diameter of the liquid jet, and the radius of the resulting droplets is approximately 1.9 times the radius of the liquid jet (Wallis, 1969). These classical solutions can readily be employed in the characterization of the length scales of the postulated liquid jets and their breakup, using the aforementioned relationships, the jet diameter and droplet diameter can be expressed as

$$D_{jet} \approx \frac{\lambda_{crit}}{4.5} \approx 0.22\lambda_{crit} \tag{16}$$

$$D_{drop} \approx 1.9 D_{jet} \approx 0.42\lambda_{crit} \tag{17}$$

The number of waves within the control volume ($N_{w,cv}$) which directly represents the number of jets within the control volume is estimated utilizing a similar methodology as was used in the development of the annular film flow droplet entrainment model by Holowach (2002), except in this case instead of a spacing equal to the Kelvin–Helmholtz wavelength, it is postulated that droplets are generated along the heated perimeter with a spacing equal to the diameter of the liquid jet. Therefore the number of droplets generated within the control volume over the characteristic control volume time period is given by

$$N_{w,cv} = \frac{P_H}{2D_{jet}} = 2.27\frac{P_H}{\lambda_{crit}} \tag{18}$$

The volume of an average droplet that is swept away by the action of the vapor flow is calculated using the diameter given by the Rayleigh criterion. The entrained droplet volume is given as

$$V_{entr,d} = \frac{4\pi}{3} r_d^3 = 0.0388\lambda^3_{crit} \tag{19}$$

In order to more easily visualize the assumed spatial characteristics for this quench front/froth front entrainment model, a figure has been constructed such that a depiction from the perspective of "looking down" into a rod bundle subchannel is given. Fig. 5 displays a top-down view into a conventional PWR rod bundle array flow subchannel, delineating the length scales, droplet sizes, and droplet spacings that are assumed in this model development.

By substituting Eqs. (9), (15), (18), and (19) into Eq. (8), an expression for the droplet entrainment mass flux (S_E) within the control volume at the top of the froth front is arrived at

$$S_E = 0.088\frac{\lambda_{crit}\rho_f P_H (U^2_{vap,crit} + U^2_{vap,bqf})^{1/2}}{2A_F} \tag{20}$$

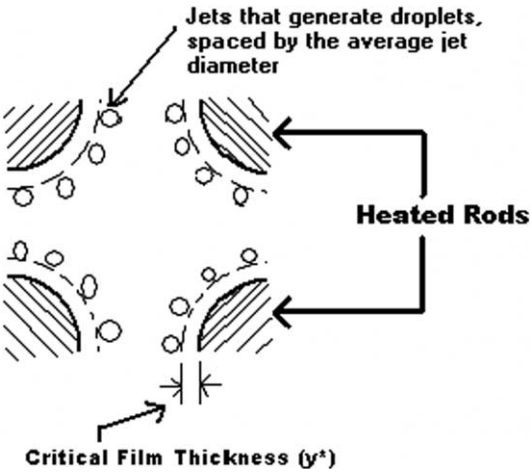

Fig. 5. Top down schematic of the postulated quench/froth front entrainment model applied to a conventional PWR flow subchannel.

Eq. (20) can be considered an estimate of the entrained droplet mass flux generated at the quench front based on the physics employed in this control volume analysis. The next step in the development of a physical model for the droplet entrainment at the top of the froth front brought on by quenching action is to compare the predictions of Eq. (20) to a range of experimental data. By comparison of the control volume analysis with experimental data, parametric dependencies can be identified, and any necessary corrections can be developed such that the accuracy of the proposed model may be upgraded to predict the droplet entrainment rate in a quench front/froth front scenario over a range of flow, energy release, and pressure conditions.

3.1. Comparison of experimental data and model-predicted droplet entrainment rates

At this point, an expression for the postulated entrainment rate at a quench front/froth front has been developed based on a fundamental analysis of the postulated transport and system response time and length scales that characterize the vapor generation at and below a quench front. The characteristic time scales were developed based on the vapor generated at and below the quench front, and the characteristic length scales were based on the critical film thickness for a vapor film that is generated by quenching action and the Kelvin–Helmholtz critical wavelength as a length scale for the characterization of the ligament deformation and breakup into droplets.

In order to develop a corrected expression for the droplet entrainment rate due to quenching over a range of conditions, a comparison of the predictions of Eq. (20) with the experimental data from University of California at Berkeley (Seban et al., 1978; Seban and Greif, 1983; Ng and Banerjee, 1983) and data from the REFLEX series of experiments conducted by the United Kingdom Atomic Energy Authority at Winfrith (Denham et al., 1980; Denham, 1981) was conducted. The data points that were selected for this portion of the model development were taken at various fluid flow conditions covering a range of pressures (0.1–0.4 MPa). The conditions of the selected data generally capture the postulated pressure range (0.1–0.4 MPa), quench flow velocities (0.01–0.15 m/s), and rod quench energy release rates (0.1–3 kw/rod) for the LOCA reflood phenomena in a PWR. The data from the fundamental tube reflood experiments were reduced so as to arrive at a range of possible droplet entrainment rates for a given set of experimental conditions as discussed in the first section of this paper and summarized in Tables 3 and 4.

The estimated experimental droplet entrainment mass fluxes (for the void fraction estimates of 0 and 1) were divided by the predicted droplet entrainment mass flux Eq. (20) so as to arrive at a range of E/P (experimental over predicted) ratios for a given set of fluid flow and energy release conditions. These respective E/P ratios were plotted with error bars to reflect the range of possible entrained mass fluxes (identified in Table 3) versus the vapor generation Reynolds number in Fig. 6. The vapor generation Reynolds number is defined in terms of the vapor generation rate, hydraulic diameter, flow area, and vapor viscosity as

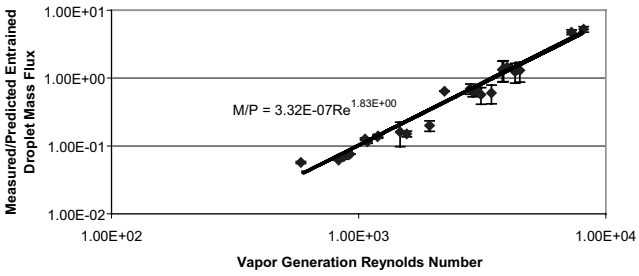

Fig. 6. Ratio of experimental to predicted droplet entrainment mass flux at the quench front.

$$Re_{\mathrm{vap,gen}} = \frac{\Gamma D_{\mathrm{H}}}{A_{\mathrm{F}}\mu_g} \tag{21}$$

The plot of the ratio of experimental to predicted (Eq. (20)) droplet entrainment mass fluxes at the quench front versus vapor generation Reynolds number given in Fig. 6 for the 24 data points examined shows a clear dependency on the vapor generation Reynolds number (Eq. (21)). This dependency of the ratio of the experimental to predicted entrainment mass flux appears to be roughly proportional to the vapor generation Reynolds number squared for the range of data examined. It is believed that the vapor generation Reynolds number serves as a correction to better account for the number of droplets generated in the control volume per characteristic time period. The postulated number of droplets generated is assumed to be able to be calculated assuming a well-ordered series around the heated perimeter separated by a dimension equal to the diameter of the liquid jet. But, in actuality, this ordering may be different, with droplets generated in various locations away from the wall. The rate of vapor generation, and its relationship to a characteristic limiting length scale (the hydraulic diameter) is modeled with the use of the vapor generation Reynolds number, hence a better estimate of the number of droplets generated can be made by utilizing this correction.

A line drawn through the error bars of the data points in Fig. 6 yields a correction to Eq. (20) such that the droplet entrainment mass flux at the quench front may be more accurately calculated. It is interesting to note that the range of vapor generation Reynolds numbers for a conventional PWR reflood transient falls approximately in the range of 2000–5000, which nearly corresponds with an experimental to predicted ratio of one. This fact is encouraging since it means that the physical model presented in the analysis leading to

Eq. (20) nearly predicts the experimental entrainment rates at prototypical quench front energy release rates, and effectively correlates data points both above and below prototypical energy release rates.

Utilizing the curve drawn in Fig. 6, a corrected and final form for the droplet entrainment mass flux at the quench front is arrived at which accounts for the parametric dependency on the vapor generation Reynolds number. The means for calculating the droplet entrainment mass flux at the top of a froth front is in a form that can be conveniently implemented into a finite difference thermal hydraulic computer code. The corrected entrainment mass flux at the top of the froth front is given by

$$S_E = C_1 \frac{\lambda_{crit}\rho_f P_H (U^2_{vap,crit} + U^2_{vap,bqf})^{1/2}}{A_F} Re^{C_2}_{vap,gen} \qquad (22)$$

In the above equation, the dimensionless constants, C_1 and C_2, were developed from the correction curve plotted in Fig. 6 and by combining constant terms, such that

$C_1 = 1.46 \times 10^{-8}$

$C_2 = 1.83$

4. Model evaluation with FLECHT-SEASET reflood test data

Several experimental test runs from the FLECHT-SEASET (Loftus et al., 1980) series of reflood tests were selected for the evaluation of the proposed reflood entrainment model. The proposed reflood entrainment model, along with upgraded annular film flow entrainment and interfacial drag models from the dissertation of Holowach (2002) were implemented into the COBRA-TF systems analysis computer code and used to compare and assess model predictions against these integral effects test data. Additionally, a comparison with the prediction of the original version of the COBRA-TF (Paik et al., 1985) code is presented to show the improvements realized in the utilization of the proposed model set.

For the purposes of the evaluation of the proposed entrainment model, three FLECHT-SEASET runs were selected for evaluation since they fairly exemplify a range of postulated reflood conditions for a typical PWR. These tests were conducted in the 161 heated rod FLECHT facility with a uniform radial power profile and chopped cosine axial power profile over the range of conditions listed in Table 5.

A single channel COBRA-TF input model of the FLECHT facility was constructed with ~0.13 m axial hydraulic nodes and variable axial thermal nodes. With the exception of node spacing, this input model closely resembled that used by Paik et al. (1985). The original COBRA-TF minimum film boiling temperature model was utilized for this series of calculations (Loftus et al., 1980).

4.1. Evaluation of clad temperature predictions

A primary means of evaluation of a quench front entrainment model is to compare the predicted and measured clad temperatures over time at various axial elevations. Such comparisons also assess the calculated location of the quench front over time with that measured in the experimental data. Since the quench front location as a function of time is strongly related to the droplet entrainment rate at the quench front, this means of comparison will serve as a first-check of the proposed entrainment model set.

Figs. 7 and 8 show the predicted and average experimentally measured clad temperatures as a function of time at axial elevations of 1.98 and 2.29 m for Run 31504. Figs. 9 and 10 show the predicted and average experimentally measured clad temperatures as a function of time at an axial elevation of 2.29 m for Runs 32013 and 31805, respectively. The bars on the experimentally measured clad temperature values indicate the range of thermocouple readings at a given axial elevation.

The results presented in Figs. 7–10 show excellent agreement with the experimentally measured clad temperatures and those calculated utilizing the upgraded version of COBRA-TF, since the predicted quench time of the clad thermocouple is quite close to the measured quench time. This observation is indicative of the code properly calculating the correct quench front velocity over time, for the range of reflood cases examined.

4.2. Liquid carryover comparison

Comparison of calculated and experimental liquid carryover from the bundle is one means to assess the

Table 5
Range of conditions for FLECHT-SEASET runs used for model evaluation

Run number	FS 31504	FS 32013	FS 31805
Upper plenum pressure (MPa)	0.28	0.41	0.28
Initial clad temperature at 1.83 m (K)	1136	1160	1144
Rod peak power (kw/m)	2.3	2.3	2.3
Cold fill rate (mm/s)	24.6	26.4	21.0
Injected coolant temperature (K)	324	339	324

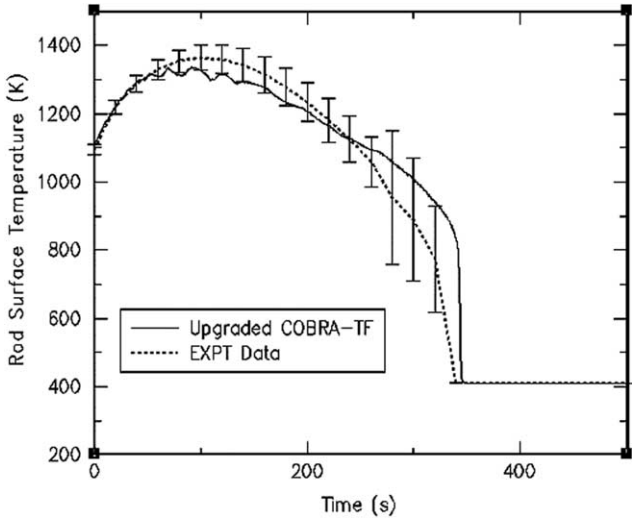

Fig. 7. Comparison of upgraded code-calculated and experimentally measured clad temperatures for FLECHT-SEASET Run 31504 at 1.98 m axial elevation.

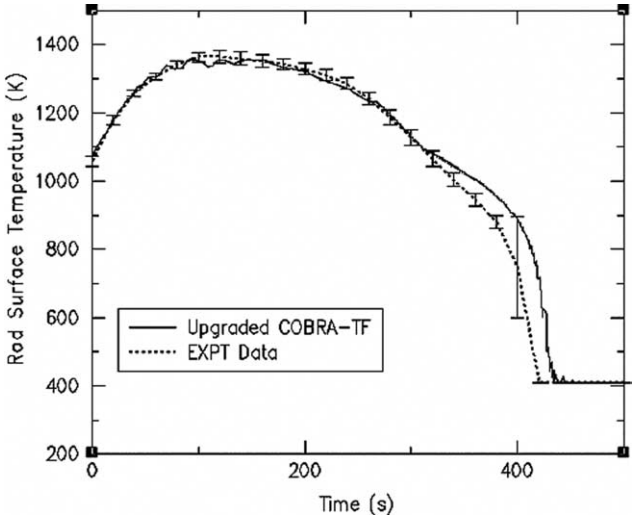

Fig. 8. Comparison of upgraded code-calculated and experimentally measured clad temperatures for FLECHT-SEASET Run 31504 at 2.29 m axial elevation.

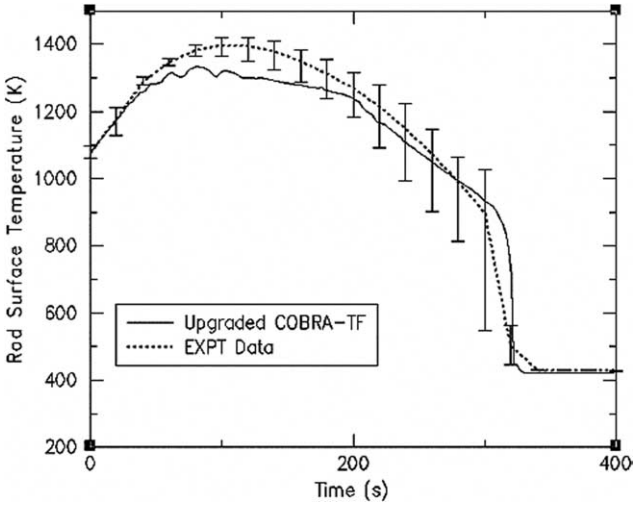

Fig. 9. Comparison of upgraded code-calculated and experimentally measured clad temperatures for FLECHT-SEASET Run 32013 at 2.29 m axial elevation.

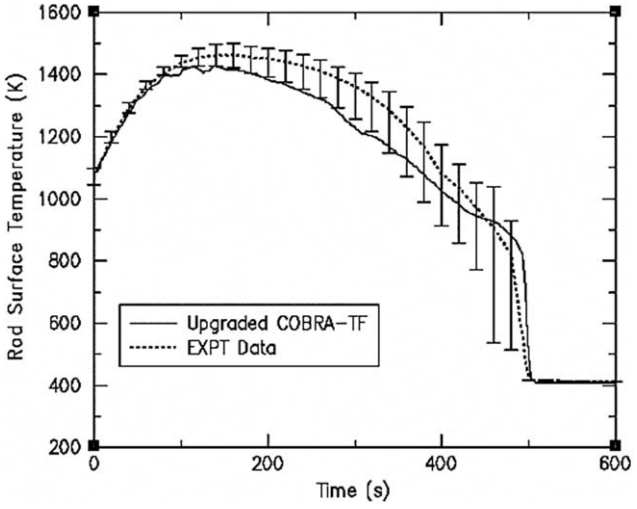

Fig. 10. Comparison of upgraded code-calculated and experimentally measured clad temperatures for FLECHT-SEASET Run 31805 at 2.29 m axial elevation.

integral effects of the droplet entrainment and interfacial heat and mass transfer models within a transient two-phase systems analysis computer code. The carryover of liquid droplets out of a test bundle reflects the mass flow rate of droplets entrained either at a quench front and/or due to film flow minus the effects of the evaporation of the liquid droplet phase due to the characteristic non-equilibrium superheated steam conditions prevalent in a rod bundle during the reflood phase.

For FLECHT-SEASET Runs 31504, 32013, and 31805, respectively, Figs. 11–13 display both the experimentally measured carryover tank level as well as the level predicted by the COBRA-TF calculation of the integral of the entrained mass flow rate exiting the bundle.

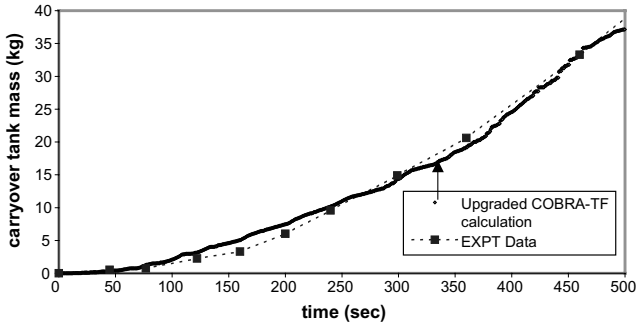

Fig. 11. Comparison of upgraded code-calculated and experimentally measured carryover tank level for FLECHT-SEASET Run 31504 as a function of time.

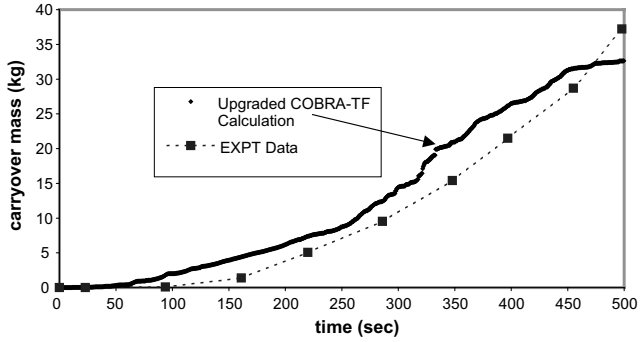

Fig. 12. Comparison of upgraded code-calculated and experimentally measured carryover tank level for FLECHT-SEASET Run 32013 as a function of time.

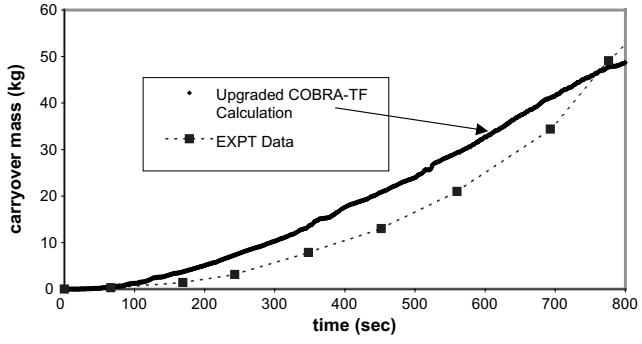

Fig. 13. Comparison of upgraded code-calculated and experimentally measured carryover tank level for FLECHT-SEASET Run 31805 as a function of time.

Figs. 11–13 generally show satisfactory agreement between the measured and code-predicted liquid carryover indicating that the integral effects of the quench front entrainment and interfacial heat/mass transfer models appear to be performing correctly. The slight over-prediction of the carryover during the course of Run 31805 (Fig. 13) could be due to the lower liquid injection rate, which, during the course of the experimental test could result in a longer period of time to wet the walls of the separator and carryover tank, thus giving a lower-than-expected carryover tank level. One must be careful in using this prediction as the only yardstick in entrainment and interfacial heat/mass transfer model evaluation, since compensating effects can occur (i.e. too much interfacial mass transfer at low elevations, and too little at high elevations, or vice versa).

4.3. Quench front location comparison

An additional means of code model evaluation is to examine the quench front location as a function of time. The progression of a quench front during a reflood transient is strongly tied to the entrainment and vapor generation rates as well as the void fraction at the quench front. Comparison of the predicted quench front location as a function of time with that of the experimental data is warranted.

Figs. 14–16 are plots of the code-predicted as well as the experimentally measured quench front location as a function of time for Runs 31504, 32013, and 31805, respectively. All cases (Figs. 14–16) show excellent agreement between the code-calculated and measured quench front locations for a majority of each reflood transient, indicating a satisfactory integral prediction of both the quench front droplet entrainment and heat transfer/vapor generation models. Some divergence between the predicted and measured quench front locations is observed in the latter portions of the transient, where top quench effects become more significant. Better quench front location results could possibly be obtained utilizing a more detailed computational model of the upper plenum which could be obtained using a larger systems analysis code such as COBRA-TRAC, or better results may be obtained by utilizing a more comprehensive

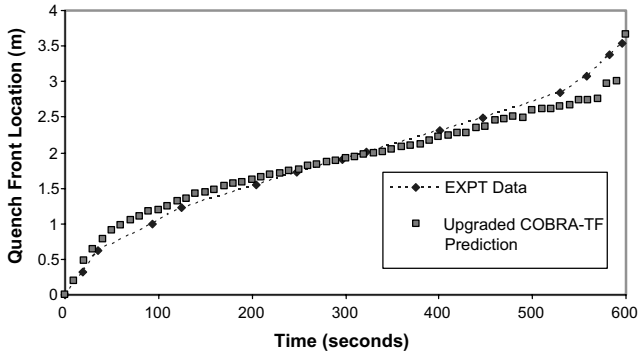

Fig. 14. Comparison of upgraded code-calculated and experimentally measured quench front location for FLECHT-SEASET Run 31504 as a function of time.

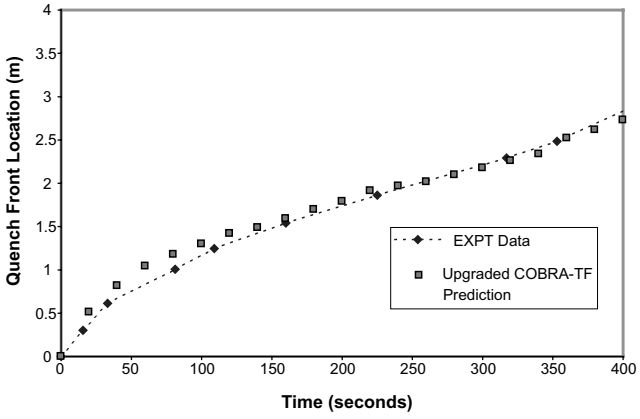

Fig. 15. Comparison of upgraded code-calculated and experimentally measured quench front location for FLECHT-SEASET Run 32013 as a function of time.

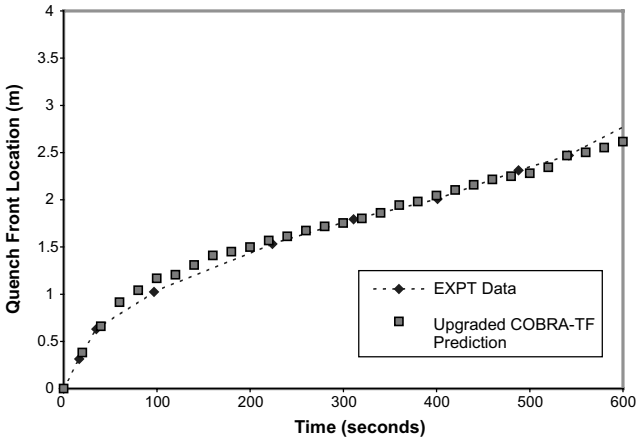

Fig. 16. Comparison of upgraded code-calculated and experimentally measured quench front location for FLECHT-SEASET Run 31805 as a function of time.

falling film interfacial drag model or top quench entrainment model. Needless to say, the agreement of the results of the quench front location as a function of time do lend credence to the predictive capability of the quench front entrainment model over a range of bundle conditions from subcooled conditions low in the bundle to highly saturated conditions high in the bundle.

4.4. Comparison of upgraded code predictions with those of the original FLECHT 163 version of COBRA-TF (Lee et al., 1982)

Detailed assessments of the deficiencies of the FLECHT 163 version of COBRA-TF (Lee et al., 1982) have been presented by Frepoli et al. (2000) and in the dissertation of Frepoli (2001). In order to further substantiate the improvements of the proposed entrainment model implemented in COBRA-TF, it is appropriate to present some comparisons of upgraded and original code calculations. Calculations of the FLECHT-SEASET Run 31504 are utilized for comparison sake to identify model improvements. More detailed comparisons and sensitivity studies confirming the viability of the new entrainment model are presented in the dissertation of Holowach (2002).

In an effort to compare code model predictions for the FS Run 31504 reflood test, it is convenient to examine the calculated wall temperature at a given axial location for two different hydraulic node size schemes. The original COBRA-TF model set was specifically developed based on the FLECHT SEASET series of reflood tests (Lee et al., 1982). The comparisons discussed below point to the model deficiencies in the original version of COBRA-TF.

Figs. 17 and 18 show the comparison of the original and upgraded COBRA-TF models sets as well as the experimentally measured clad temperatures at the 2.29 m

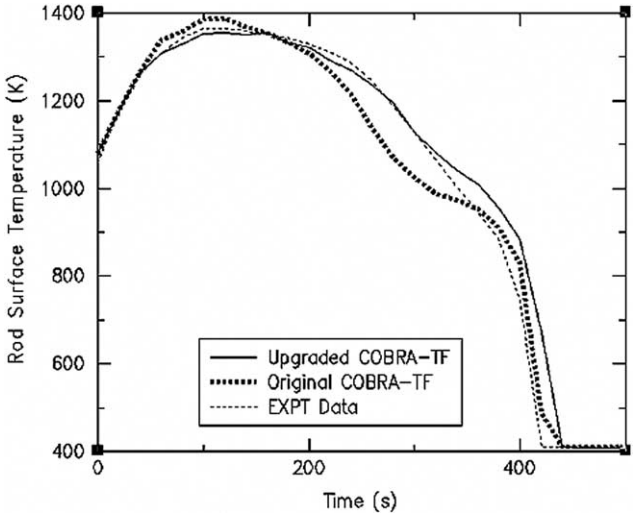

Fig. 17. Comparison of upgraded code-calculated, original code-calculated, and experimentally measured clad temperatures for FLECHT SEASET Run 31504 at 2.29 m axial elevation for a ~0.13 m hydraulic node spacing.

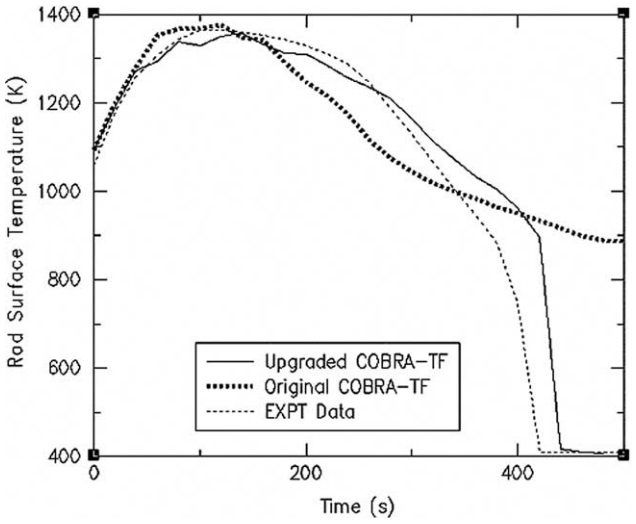

Fig. 18. Comparison of upgraded code-calculated, original code-calculated, and experimentally measured clad temperatures for FLECHT SEASET Run 31504 at 2.29 m axial elevation for a ~0.25 m hydraulic node spacing.

axial elevation as a function of time for the ~0.13 and ~0.25 m hydraulic node spacing, respectively.

Fig. 17 shows a relatively satisfactory prediction of the 2.29 m clad temperature by the original version of COBRA-TF, but, consistent with the observations of Frepoli et al. (2000), altering the node size has a significant effect on the clad temperature prediction and quench characteristics, as can be seen in Fig. 18. When the node size is increased for the original COBRA-TF code, the code fails to predict a quench of the 2.29 m axial location, which is indicative of an entrainment model deficiency where too high of an entrainment rate

is predicted thus "stalling" the quench front. This drastic effect on clad temperature and quench time is not seen in the upgraded code model. Using the new models described in this paper, similar quench times are observed for both a fine and coarse hydraulic node size scheme.

The results of the comparison of the original FLECHT 163 version of COBRA-TF (Lee et al., 1982) with that of the upgraded version of the code presented in this work clearly show the improvement in hydraulic node-size sensitivity issues due to the proposed model's primary dependency on energy release rates where the quench front entrainment rate model in the FLECHT 163 version of COBRA-TF is tied to a local void fraction dependency which is calculational cell size-dependent. Good calculational predictions over a range of hydraulic node sizes add more credence to the stability and basis of the quench front droplet entrainment model developed in this paper, as well as making it more useful for complex system analysis.

5. Conclusions

A model for calculating the mass flux of entrained liquid droplets at a quench front has been developed by a process of first reducing a series of fundamental test data and developing a postulated physical model based on characteristic time and length scales. Then, by the comparison of a postulated physical model with the reduced test data, the physical model was corrected to account for parametric dependencies. Upon plotting the ratio of the experimental to physical model-predicted entrainment rates, a correction related to the vapor generation rate was arrived at to fine-tune the physical model to better represent the actual experimental data. This model has been developed over a range of data to include pressures, flow rates, and energy release rates that encompass prototypical parameters characterizing a conventional PWR reflood scenario.

It should be noted that the proposed model set tends to under-predict droplet size, so, it was necessary to continue to utilize the FLECHT-163 COBRA-TF (Paik et al., 1985) droplet size correlation for the code calculations performed. Therefore the model set proposed in this section is primarily used to predict the entrainment mass flow rate at the quench front. More detailed jet stability and breakup analyses with the use of advanced droplet size data such as that from the Penn State Rod Bundle Heat Transfer (RBHT) program (Hochreiter et al., 1998), could lead to a further improvement in this model set such that it may be used for actual droplet size prediction.

The model was implemented into the COBRA-TF finite difference thermal hydraulic systems analysis computer code, so as to utilize the code to predict independent sets of integral transient test data not used in the model development process. The prediction of several sets of the FLECHT SEASET rod bundle reflood experiments utilizing the upgraded COBRA-TF code shows that the proposed quench front entrainment model performs satisfactorily over a range of prototypical reflood conditions, and can be a great benefit for improving advanced safety analysis predictive capabilities. Additionally, the proposed quench front entrainment model shows a limited sensitivity to calculational hydraulic node size, which adds important flexibility and confidence in the performance of complex system calculations.

References

Denham, M., 1981. Heat Transfer Near The Quench Front in Single Tube Reflooding Experiments, AEEW-R-1436, Atomic Energy Establishment, Winfrith, England.

Denham, M.K., Elliot, D.F., Shawyer, K.J., 1980. Fundamental Studies of the Reflooding of an Inconel Tube in the REFLEX Rig, AEEW-R 1353, Reactor Development Division, AEE, Winfrith, Dorchester.

Frepoli, C. et al., 2000. A noding sensitivity analysis using COBRA-TF and the effect of spacer grids during core reflood, in: Proceedings of ICONE-8—8th International Conference on Nuclear Engineering, Baltimore, MD.

Frepoli, C., 2001. Development of a Subgrid Model with a Fine Moving Grid Overlying a Coarse Eulerian Mesh for Modeling Reflood Heat Transfer, Ph.D. Dissertation, The Pennsylvania State University Department of Mechanical and Nuclear Engineering.

Hewitt, G., Hall-Taylor, N., 1970. Annular Two-Phase Flow. Pergamon Press, New York.

Holowach, M.J., 2002. A Physical Model for Predicting Droplet Entrainment in Transient Two-Phase Fluid Flow and Heat Transfer Systems Analysis Computer Codes, Ph.D. Dissertation, The Pennsylvania State University Department of Mechanical and Nuclear Engineering.

Holowach, M.J., Hochreiter, L.E., Cheung, F.B., 2002. A model for droplet entrainment in heated annular flow. International Journal of Heat and Fluid Flow 23 (6), 807–822.

Hochreiter, L. et al., 1998. Rod Bundle Heat Transfer PEER Report, PSU ME/NE—NRC-04-98-041 Report 1, The Pennsylvania State University Department of Mechanical and Nuclear Engineering.

Hsu, Y.Y., Westwater, J.W., 1960. Approximate theory for film boiling on vertical surfaces, in: Chemical Engineering Progress Symposium Series, Heat Transfer—Storrs, CT, vol. 56, no. 30, pp. 15–24.

Ishii, M., Grolmes, M., 1975. Inception criteria for droplet entrainment in two-phase concurrent film flow. AIChE Journal 21 (2), 308–318.

Kataokoa, I., Ishii, M., 1983. Mechanistic Modeling and Correlations for Pool Entrainment Phenomenon, NUREG/CR-3304, ANL-83-87.

Lee, N., Wong, S., Yeh, H.C., Hochreiter, L.E., 1982. PWR FLECHT SEASET Unblocked Bundle, Forced and Gravity Reflood Task Data Evaluation and Analysis Report, EPRI NP-2013/NUREG CR-2256/WCAP 9891, Westinghouse Electric Corporation, Monroeville, PA.

Loftus, M. et al., 1980. PWR FLECHT SEASET Unblocked Bundle, Forced and Gravity Reflood Task Data Report, NRC/EPRI/Westinghouse Report no. 7, NUREG/CR-1532, EPRI NP-1459/WCAP-9699.

Ng, Y., Banerjee, S., 1983. Two-Phase Flow Characteristics During Controlled Oscillation Reflooding of a Hot Vertical Tube, EPRI NP-2821.

Paik, C.Y., Hochreiter, L.E., Kelly, J.M., Kohrt, R.J., 1985. Analysis of FLECHTSEASET 163 Rod Blocked Bundle Data Using COBRATF, NUREG/CR4166, WCAP 103 75, EPRINP41 11.

Rohsenow, W.M., Webber, J.H., Ling, A.T., 1953. Effect of vapor velocity on laminar and turbulent-film condensation. Transactions of the American Society of Mechanical Engineers 78, 1637–1643.

Seban, R.A. et al., 1978. UC-B Reflood Program: Experimental Data Report, EPRI NP-743, University of California at Berkeley.

Seban, R., Greif, R., 1983. Reflooding of a Vertical Tube at 1, 2, and 3 Atmospheres, EPRI NP-3191.

Wallis, G., 1969. One-Dimensional Two-Phase Flow. McGraw-Hill, New York.

Woodmansee, D., Hanratty, T., 1969. Mechanism for the removal of droplets from a liquid surface by a parallel air flow. Chemical Engineering Science 24, 299–307.